Developmental Cell
Article

Genetic Control of Plant Development by Overriding a Geometric Division Rule

Saiko Yoshida,[1,5] Pierre Barbier de Reuille,[2,5] Brendan Lane,[3] George W. Bassel,[4] Przemyslaw Prusinkiewicz,[3] Richard S. Smith,[2,6,*] and Dolf Weijers[1,*]
[1]Laboratory of Biochemistry, Wageningen University, Dreijenlaan 3, 6703HA Wageningen, the Netherlands
[2]Institute for Plant Sciences, University of Bern, Altenbergrain 21, Bern 3013, Switzerland
[3]Department of Computer Science, University of Calgary, Calgary, AB T2N 1N4, Canada
[4]School of Biosciences, University of Birmingham, Birmingham B15 2TT, UK
[5]Co-first author
[6]Present address: Department of Comparative Development and Genetics, Max Planck Institute for Plant Breeding Research, Carl-von-Linne-Weg 10, 50829 Köln, Germany
*Correspondence: smith@mpipz.mpg.de (R.S.S.), dolf.weijers@wur.nl (D.W.)
http://dx.doi.org/10.1016/j.devcel.2014.02.002

SUMMARY

Formative cell divisions are critical for multicellular patterning. In the early plant embryo, such divisions follow from orienting the division plane. A major unanswered question is how division plane orientation is genetically controlled, and in particular whether this relates to cell geometry. We have generated a complete 4D map of early *Arabidopsis* embryogenesis and used computational analysis to demonstrate that several divisions follow a rule that uses the smallest wall area going through the center of the cell. In other cases, however, cell division clearly deviates from this rule, which invariably leads to asymmetric cell division. By analyzing mutant embryos and through targeted genetic perturbation, we show that response to the hormone auxin triggers a deviation from the "shortest wall" rule. Our work demonstrates that a simple default rule couples division orientation to cell geometry in the embryo and that genetic regulation can create patterns by overriding the default rule.

INTRODUCTION

The generation of a functional body pattern from a single embryonic cell requires the spatially coordinated acquisition of different cell identities, and hence formative divisions that give rise to new cell types or layers are important drivers of morphogenesis (De Smet and Beeckman, 2011). However, underlying mechanisms are poorly understood and a central question is how formative divisions differ from proliferative ones. The plant embryo is an ideal system for addressing this question, as it is a growing three-dimensional (3D) structure where patterning emerges de novo. Starting from a single, axis-symmetric cell attached to a suspensor, cell division patterns in *Arabidopsis* embryogenesis appear almost invariant (Jürgens and Mayer, 1994; Scheres et al., 1994), making development highly predictable. Because cell walls prevent migration, division plane orientation is an important determinant of pattern formation. Regulators of plant embryo patterning have been identified through genetics, and mutations often alter the stereotypical orientation of formative divisions (Mayer et al., 1991; Tzafrir et al., 2004). Interpretation of abnormal development, and hence the cellular function of pattern regulators, is challenging, however, as the cellular basis for oriented cell division is not known. One particular limitation is that, while development occurs in three spatial dimensions, (optical) 2D sections of embryos are used to define cellular shapes and division patterns. As cells can have complex, polyhedral shapes, these are not always easily inferred from sections, and hence our view of the effect of mutations on cell shapes and division plane control are inherently inaccurate. The recent development of 3D imaging and cellular segmentation approaches has given a more detailed insight in relative arrangements of cells (Bougourd et al., 2000; Truernit et al., 2008; Federici et al., 2012) and shape changes during organogenesis (Fernandez et al., 2010; Lucas et al., 2013). The application of this approach to the highly predictable early embryo in principle should enable the study of the individual cellular basis for oriented growth and division in a multilayered, 3D context.

Importantly, the highly predictable divisions in the early embryo should allow addressing of the central question of how genetic regulation interacts with geometric cues to orient division planes. For more than a century, botanists have formulated hypothetical "rules" underlying oriented cell division (summarized in Kwiatkowska, 2004). Hofmeister (1863) suggested that new wall appears perpendicular to the principal direction of growth, whereas Sachs suggested that newly inserted walls should intersect existing walls at 90 degrees (Sachs, 1878). Errera's rule states that the new division wall is a surface of minimum energy (Errera, 1888), drawing an analogy with soap bubbles. However, no deterministic rule for cell division is able to match cell division patterns exactly, and Besson and Dumais (2011) have extended Errera's rule to include the inherent stochasticity of cell division. Besson and Dumais (2011) showed that a rule based on the competition between local minima in energy is able to predict observed division patterns in a wide range of land plants and algae and proposed it as a general rule for

symmetric cell division in plants. The rule also has a solid molecular basis, with a plausible mechanism explaining the division orientation proposed (Lloyd, 1991). In simulation models, the rule is often approximated as the shortest wall passing through the center of the cell (Dupuy et al., 2010; Smith et al., 2006; Stoma et al., 2008), although even here a stochastic component to the positioning of the cell center has been suggested to generate more representative cell division patterns (Nakielski, 2000; Sahlin and Jönsson, 2010). While these widely accepted rules offer an intuitive framework for rationalizing cell division planes, it is important to note that manifestations of these rules have so far been tested only in 2D. Therefore, it is not clear whether such a simple rule can explain division planes in complex 3D cell shapes, let alone explain the establishment of a patterned, 3D embryo. Finally, if "default" geometric rules underlie cell division orientation in the embryo, an important question is how genetic control operates to drive formative divisions. In particular, an outstanding question is how the changes in division planes that are induced by mutations in pattern regulators relate to this geometric framework. Here, we have addressed this problem by first generating a four-dimensional reconstruction of the formative events during early *Arabidopsis* embryo development. We use computational approaches and genetic perturbation to explore the roles of geometry and genetic regulation on cell division and show that the plant hormone auxin controls pattern formation by overriding a default geometric division rule.

RESULTS

Analysis of Cellular Patterns in 3D

Plant embryos are encapsulated in seed and fruit and this, along with their small size (Figure 1A), poses challenges in imaging. Traditionally, embryos have been analyzed by optical microscopy of entire seeds (Figure 1B and Figure S1A available online) or by 2D sections (Figure S1B). To accurately analyze cell volumes and division planes in 3D, we adapted a procedure for fluorescent staining of fixed embryos (Truernit et al., 2008) and performed high-resolution confocal imaging followed by the segmentation of cell volumes (Figure 1C). These volumes are likely accurate as the imaging procedure itself imposed very limited deformation of spherical beads (Figure S2A). Furthermore, the cell wall staining procedure does not induce artifacts, as segmentation of live embryos, visualized using a fluorescent membrane dye, gave identical results (Figure S2B). We next generated a complete series of embryo stages up to the late heart stage, thus capturing all formative events of embryogenesis (Figures 1D–1F).

In many animals, the zygote first undergoes a series of rapid cleavage divisions that partition the original cell volume before further growth increases embryo volume (Kimmel and Law, 1985; Mulnard, 1967), and based on 2D observations a similar mode has been suggested in *Arabidopsis* (Mansfield and Briarty, 1991). To determine if *Arabidopsis* embryogenesis follows an analogous pattern, we measured cellular and embryo volumes from the 1-cell to early globular stage (Figure 2A). We found that the volume of individual cells rapidly decreases from 1-cell to 8-cell stage (Figure 2A; decrease ~4-fold). After 8-cell stage, cell volume remained almost constant. In contrast, the overall embryo volume increased only by ~2-fold up to the 8-cell stage and steeply increased at later stages (Figure 2A). This suggests that the first divisions in the *Arabidopsis* embryo partition the original volume with only limited expansion, superficially analogous to cleavage divisions in several animal species. Subsequently, this switches to a distinctly different mode of growth from 8- to 16-cell stage, where the contribution of expansion to overall growth increases.

In the *Arabidopsis* embryo, early stages are named after the number of cells in the pro-embryo (1-cell through 16-cell; Jürgens and Mayer, 1994), and the discrete identification of 2-, 4-, 8-, and 16-cell stages suggests that cell divisions may be synchronized. This prediction has not been substantiated, but intermediate stages have not been reported. By observation in 3D, we found embryos with intermediate cell numbers (Figure 2B, inset), which suggests that synchronization might not be absolute. We segmented and counted cell numbers in >200 randomly isolated wild-type embryos. Cell numbers showed a clear peak at the "canonical" stages, while the population of the intermediate stages was very low (Figure 2B). Thus, we conclude that cell divisions during early embryo development may indeed be synchronized up until the 16-cell stage. However, the occurrence of intermediate cell numbers demonstrates that synchronization is not absolute.

Another key question in plant embryogenesis is how deterministic the cell division patterns are. While regenerative properties allow reconstruction of near-normal body patterns from altered cellular templates (e.g., Sena et al., 2009), the high level of regularity of cell divisions during normal development suggests some degree of determinism. Indeed, fate mapping suggested that the lineages giving rise to the two cotyledons arise very early during embryo development, possibly in the 2- to 4-cell stage (Saulsberry et al., 2002). As the two cotyledons are invariably positioned relative to the medio-lateral seed axis at later stages, we analyzed whether the first embryonic division might contribute to positioning the two cotyledon lineages. Therefore, we quantified the orientation of the first embryonic division relative to the axis of seed symmetry in cross-section and found this orientation to be preferentially orthogonal to the plane of symmetry of the ovule (Figures 2C and 2D). As the shape of the embryo-surrounding cavity is almost radially symmetric (Figure 2C), it is unclear what mechanisms might underlie the orientation of this division. However, this suggests early determinism in orienting the embryo within the seed.

Geometric Asymmetry Predicts Differential Cell Specification

Development heavily relies on differential specification, where two daughter cells are not equal in gene expression and protein accumulation (Knoblich, 2008), and one mechanism that may give rise to such differences is geometric asymmetry during division. In the context of cell division, we use the term asymmetric to denote a difference in volume of daughter cells and the term differential when speaking of cell fate. To investigate the relationship between asymmetric division and cell identity, we quantified cellular volumes (Figures 3A–3D) and compared pairs of daughter cells (Figure 3E) in a large number of randomly sampled embryos. Based on this analysis, the first two cell divisions were symmetric (Figure 3E; data not shown), but these were followed

Figure 1. *Arabidopsis* Embryo Development in 3D

(A) *Arabidopsis* embryos (heart and globular stage; lower right corner) and immature seed (containing globular stage embryo), shown alongside a human hair for size reference.

(B) Differential Interference Contrast (DIC) image of cleared globular stage embryo inside an immature seed.

(C) Procedure of cellular segmentation in MorphoGraphX. A series of optical sections, 100 nm apart, is taken through an embryo of which cell walls are fluorescently stained. These are merged into a z-stack, in which the cellular segmentation algorithm detects cellular volumes in a mesh. Cell volumes can be visualized separately, and virtual section can be made.

(D–F) Surface view (D) and longitudinal (E) and transverse (F) cross-section of *Arabidopsis* embryos. From left to right: zygote, 1-cell, 2-cell, 4-cell, 8-cell, 16-cell, early globular, mid globular, late globular, transition, early heart, and late heart stage. Cells in (D) are colored randomly, while in (E) and (F) cells are colored according to their lineage, as indicated in the color legend in (E).

Scale bars represent 100 µm in (A) and 10 µm in (D)–(F). See also Figure S1.

by two rounds of asymmetric division (Figures 3A–3E). While upper tier (Figure 3D) cells in the 8-cell stage were slightly but significantly smaller than lower tier (Figure 3D) cells, outer cells in the 16-cell stage (Figure 3D) were more than twice the volume of the inner cells (Figure 3E). This is counterintuitive as the division plane ran approximately through the center, making these

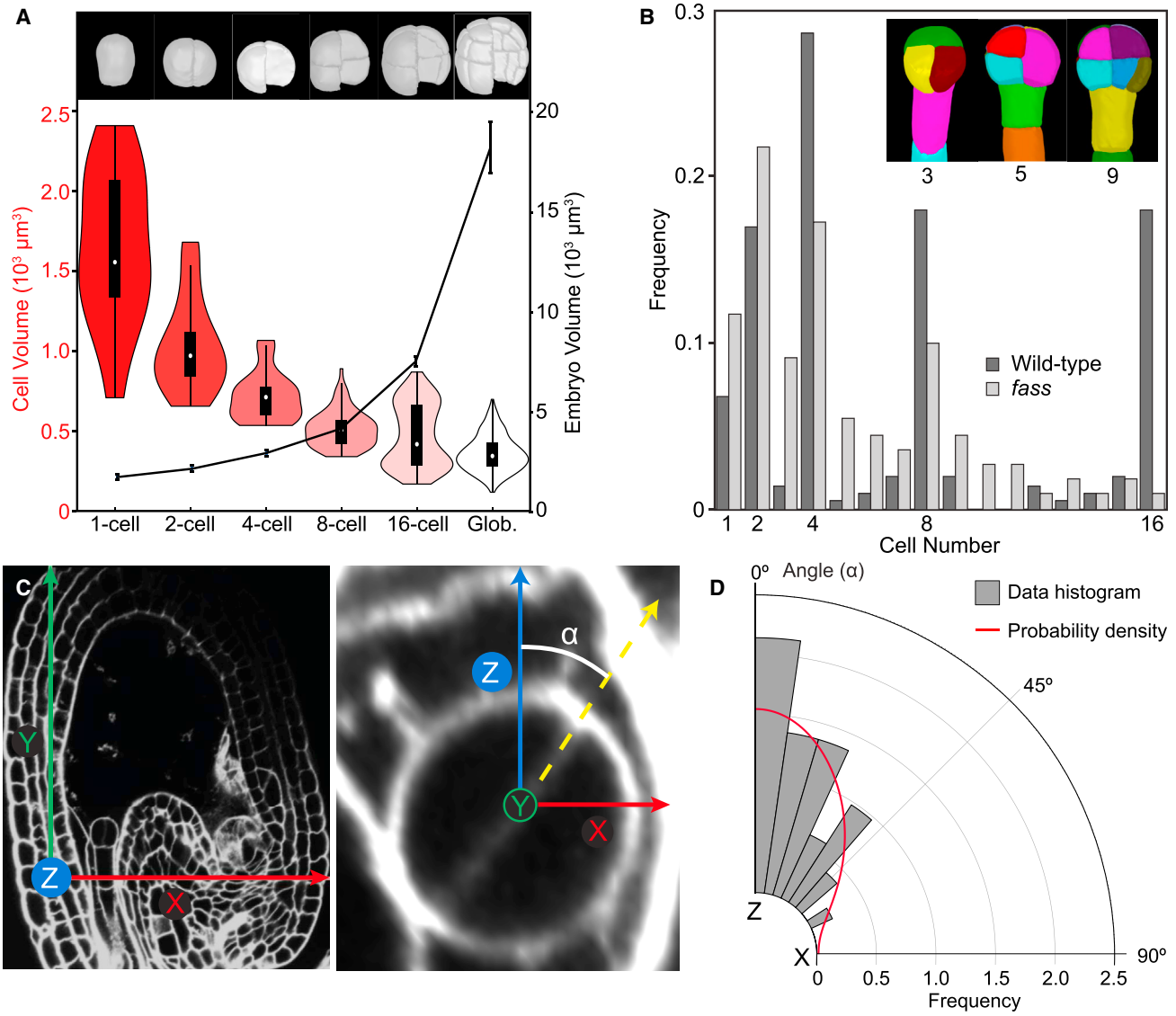

Figure 2. Nonrandom Progression, Volume, and Orientation of Early Embryogenesis

(A) Volumetric changes of whole embryo (line graph, right y axis) and embryonic cells ("violin" plots, left y axis) from 1-cell to globular stage. The width of each "violin" reflects distribution of values, and the "violin" spans from the lowest to the highest value. The thick black lines indicate the range between the first and the third quartile, and the white circle marks the median. More than ten embryos were used at each stage.

(B) Frequency distribution of embryonic stages (as cell numbers on x axis) in wild-type (dark gray; n = 206) and *fass* mutant (light gray; n = 110) embryos from 1- to 16-cell stages. Canonical stages are indicated as numbers. Inset shows wild-type embryos at intermediate stages, with cell numbers indicated.

(C) Orientation of first division of the embryo. Ovules with 2-cell-stage embryos were aligned with x, y, and z axes oriented such that the z axis was perpendicular to the micropylar-chalazal axis of the ovule, and the y axis was parallel to the division plane of the apical cell of the embryo. The angle (α) between the plane of the first cell division and the z axis was measured in the (x, z) plane.

(D) Frequency distribution of the observed orientations of the first division wall (n = 34 embryos) relative to the z axis (0°) and the x axis (90°). The red line marks the estimated density of probability of the orientation of the division wall.

See also Figure S2.

asymmetries impossible to detect in 2D sections (Figure S1B). The same volume ratio was found in segmented live embryos and in newly divided cells in embryos intermediate between 8- and 16-cell stage (Figure S2B), ruling out a significant influence by postmitotic expansion. In following stages, divisions in the upper hemisphere were very different from the lower hemisphere (e.g., Figure 3F). While both the orientation of the cell division plane and the volumetric asymmetry were extremely regular in the lower embryo hemisphere (Figure 3F), this was less constrained in the upper half (Figure 3F). Therefore, we focused our analysis on the lower part, in which cell identities are also well defined for all cells (Figures 1E, 1F, and 3D; Scheres et al., 1994).

At the transition from the 16-cell to the early globular stage, the next division round in the lower tier was asymmetric in both outer and inner cells. Outer cells generated a larger apical and smaller

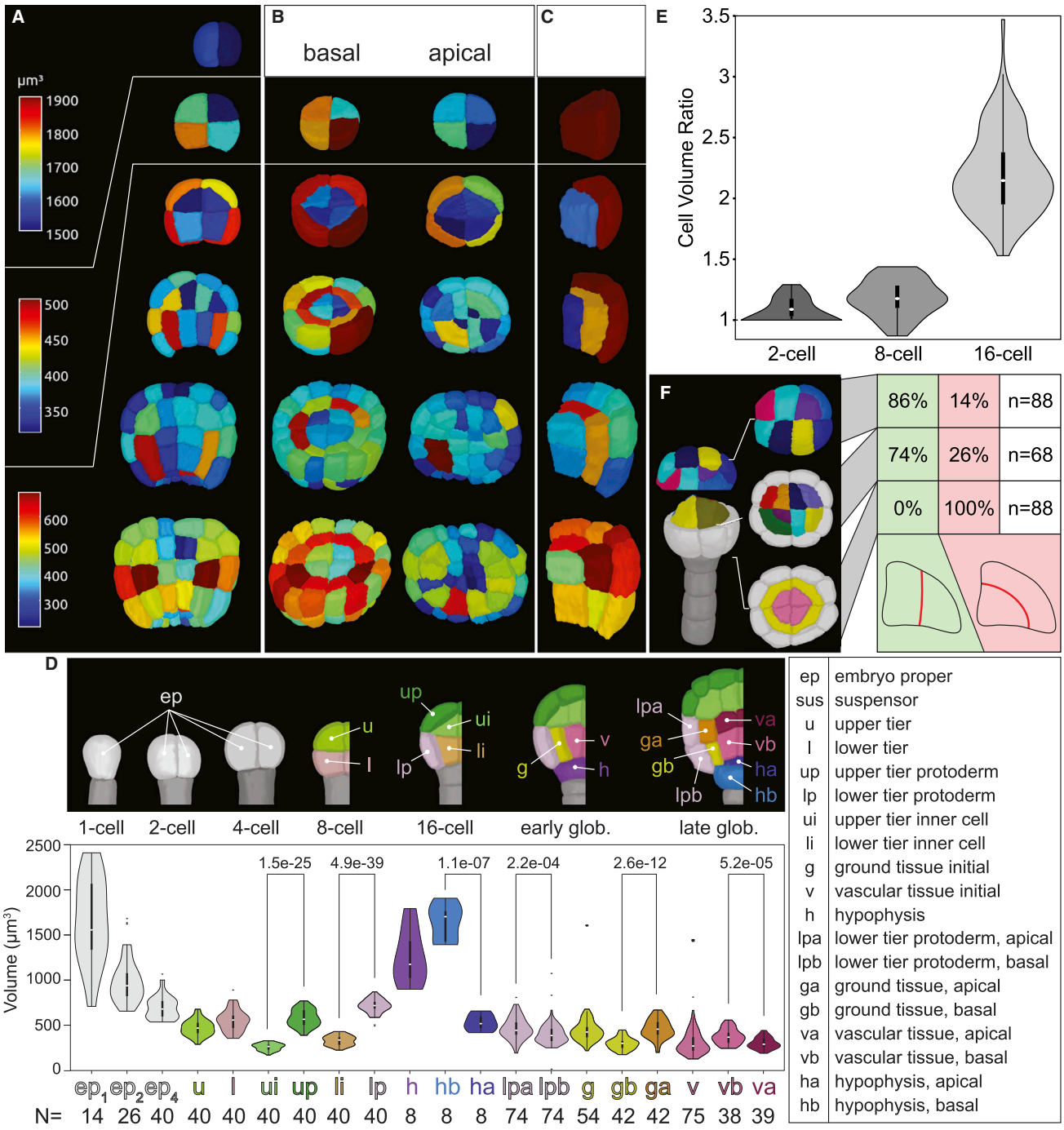

Figure 3. Cell Volumes Reveal Asymmetric Divisions

(A–C) Cellular volumes in longitudinal (A) and radial (B) cross-sections of 2-cell, 8-cell, 16-cell, early globular, mid globular, and late globular stage embryos, as well as individual cell clusters (C). Volumes are expressed as false colors according to the scales in (A) (left). The upper two embryos have their own scale, while the same scale is used for the lowest four stages.

(D) Average cell volumes (N = number of cells) in different cell types. Distributions of values are depicted as violin plots with the average indicated as a white dot and the values between the first and third quartile as a thick black line. Outliers are marked by asterisks. All unique cell types (x axis) are marked by a code in the scheme in the top. Full names of cell types are listed in the right panel. Also, p values (unpaired Welch's t test) are given for comparisons between average cell volumes.

(E) Cell volume ratio distribution between two sister cells at 2-cell, 8-cell (mean = 1.18), and 16-cell (mean = 2.21) stage (n = 13, 34, and 64, respectively). Error bars represent SEM.

(F) Cell division pattern in apical, central, and basal layers of early globular embryo (left). Cells in apical and central layers are colored randomly, while the basal tier is colored according to identity (pink, vascular; yellow, ground tissue; white, protoderm). Table shows the distribution (%) of the two cell division patterns observed. See also Figure S3.

basal cell (Figures 3A and 3D), while the inner cell generated a larger, outer ground tissue precursor (Figure 3D) and a smaller, inner vascular precursor (Figures 3A, 3C, and 3D). Subsequently, ground tissue precursors divided longitudinally (Figures 3B and 3C), while vascular precursors divided transversely (Figures 3A and 3C). Next, ground tissue cells also divided transversely. Interestingly, while longitudinal divisions were either symmetric or asymmetric (Figure 3B), transverse divisions were invariably asymmetric (Figures 3A, 3C, and 3D). The polarity of asymmetric transverse divisions depended on tissue identity; divisions in vascular precursors gave rise to larger basal cells, while those in ground tissue and protoderm produced larger apical cells (Figures 3A–3D).

None of these previously undetected asymmetric divisions were obvious in 2D sections, and in some cases such sections even suggested opposite asymmetry. For example, in both the divisions giving rise to protoderm and inner cells at the 8-cell stage and those giving rise to vascular and ground tissue precursors, the outer cell appears either equal to or smaller than the inner cell. Yet 3D analysis demonstrates that in both cases the outer cell is significantly larger.

All obligate asymmetric divisions were accompanied by differences in gene expression between the two daughter cells as reported by gene expression markers (Figure S3), while symmetric divisions produced cells of equal fate. Hence, this analysis identifies a set of asymmetric divisions during early embryogenesis and shows that asymmetric cell division strongly correlates with differential identity of the daughter cells.

Patterning by Deviations from a Default Division Rule

We next asked whether cell division in the embryo follows a default rule approximated by the minimal surface area of constant curvature (Errera, 1888), or how it may differ. A model of cell division was created that was capable of using shapes of actual cells segmented from microscopic images. When analyzing division patterns in 3D, we noticed that walls in the early embryo appear very flat in 2D cross-sections (Figures 4A–4C). To more precisely determine the shape of internal walls, we measured local maximum curvature. Curvature of the youngest walls in segmented live embryos was indeed close to zero (Figures 4D and 4E). This suggests that the new walls are accurately represented as a flat surface. Hence, we implemented the 3D equivalent of the ''shortest wall'' rule by finding the plane of minimal area passing through the geometric center of the cell. We then compared actual division planes to potential division planes found by the shortest wall rule. In this analysis we used a stochastic approach and also considered local minima (Figures 4F, 4G, and 5A), as previously implemented in 2D (Besson and Dumais, 2011). This analysis showed that while the divisions leading to the 4-cell and 8-cell stages were using the shortest wall rule (Figure 5A), those giving rise to the 16-cell stage do not correspond to a minimum, even local, at least if only planar division walls are considered. At the 2-cell stage, the cell aspect ratio was such that the difference between the division walls of largest (vertical) and smallest (horizontal) area was only about 5%. Interestingly, the divisions that avoided the global minimum were highly asymmetric (Figure 5A). To test whether this deviation from the default rule is a consequence of genetic regulation, we looked for mutants where such regulation might be perturbed, that is, mutants that revert back to the shortest wall rule.

Many embryo-defective mutants have been reported (Mayer et al., 1991; Torres-Ruiz and Jürgens, 1994; Tzafrir et al., 2004), and using our approach such defects can be visualized in 3D (Figures 5B–5E and S4). While very few of these mutants show discrete changes in the pattern of cell division, mutations in the AUXIN RESPONSE FACTOR5/MONOPTEROS (ARF/MP; Hardtke and Berleth, 1998) and its inhibitor IAA12/BODENLOS (BDL; Hamann et al., 2002) cause a distinctive switch from vertical to horizontal division in the 1-cell embryo (18% of embryos in heterozygous *BDL/bdl* background according to Hamann et al., 1999), and our analysis suggests that this represents a switch from regulated division to the shortest wall (Figure 5A). Auxin response is highly genetically buffered, and several other *ARF* genes are expressed at this stage of development (Rademacher et al., 2011). To test if auxin response alters the division program in other cells in a similar way, we ubiquitously misexpressed a nondegradable version of bdl (*RPS5A* ≫ *bdl*) that nonspecifically inhibits ARFs and thus generically suppresses transcriptional auxin response (Rademacher et al., 2012). Misexpression of bdl using this strategy causes strong auxin-insensitive phenotypes during later stages, including loss of root and cotyledon initiation and suspensor-derived embryogenesis (Rademacher et al., 2012). While early defects as observed in *bdl* or *mp* mutant embryos could not be efficiently induced with this transgenic approach, at the 8- to 16-cell transition, nearly all cells divided abnormally (Figures 5C and S4; 98.8%, n = 172 cells; wild-type: 0%, n = 160 cells). Instead of the regular division that separates the inner and outer cells that create the protoderm (Figures 1D and 1E), cells switched to a wall that was best approximated by the shortest wall rule (Figure 5A). In addition, cell divisions became nearly symmetric (Figure 5A). Therefore, we hypothesize that auxin response prevents the default shortest wall rule as defined by cell shape, forcing the cell to choose another division wall. To test whether this mechanism also operates in cells with a very different shape, we analyzed division orientation in the uppermost extraembryonic hypophysis cell (Figure 3D), which has been shown to also depend on auxin response (Rademacher et al., 2012). We found that while the normal asymmetric division follows a wall approximating the longest one (Figure 5A), cell division orientation in *RPS5A* ≫ *bdl* embryos switched to a much shorter, local minimum and created two daughters of equal volume (Figure 5A). This result strongly suggests that transcriptional auxin response is required to prevent the default shortest wall rule in several cell types of varying geometry. To substantiate this finding, we analyzed cell divisions in the *gnom* mutant (Mayer et al., 1993). *GNOM* encodes a guanine exchange factor for small ARFs and is required for polar localization of the PIN1 auxin efflux facilitator (Steinmann et al., 1999). The *gnom* mutant shows a complex phenotype that strongly correlates with reduced auxin accumulation in basal embryo regions and ectopic auxin accumulation in the embryo apex (Wolters et al., 2011). Consistent with the altered auxin response in this mutant, we found divisions consistent with the shortest wall at the 8- to 16-cell transition (Figures 5D and S4). This phenotype is specific, as a mutation in the *WRKY2* gene (Ueda et al., 2011) that gives a macroscopic phenotype similar to that of *gnom* (Figures 5D, 5E, and S4), but

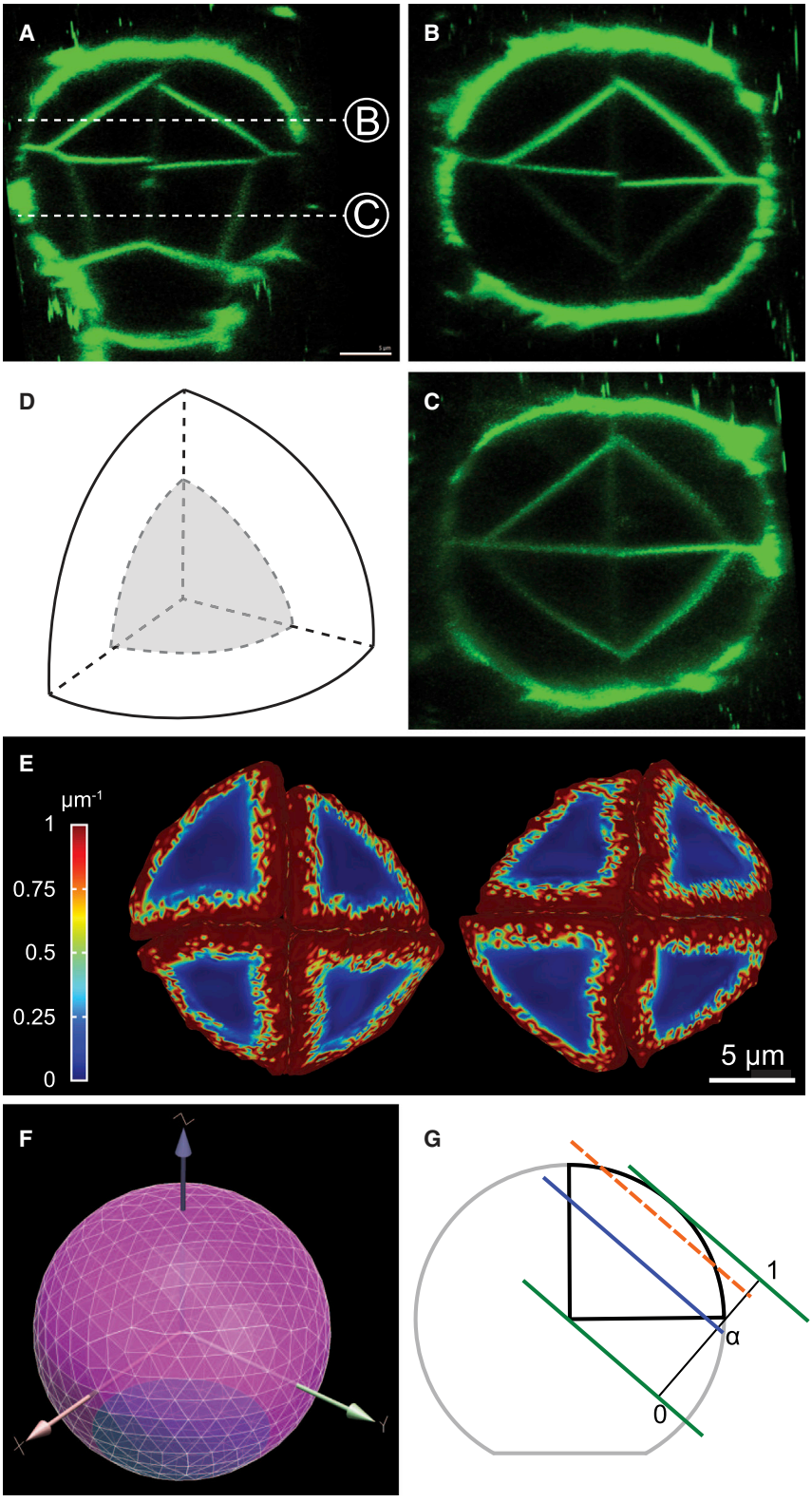

Figure 4. Planarity of Newly Formed Cell Walls and Model Description

(A–C) Longitudinal (A) and transverse (B and C) cross-sections of stained (FM4-64) live 16-cell embryos. Transverse planes in (B) and (C) are indicated in (A).

(D) 3D representation of sister cell pair in the upper hemisphere.

(E) Representative examples of maximum curvature plots of periclinal cell walls, extracted from segmented live embryos and as indicated in gray in (D). Curvature (μm^{-1}) is plotted on a false color scale, with 0 curvature being blue. For comparison, a sphere of radius 5 μm (e.g., about the size of the inner cell) has a maximum curvature of 0.2 μm^{-1}.

(F) Discretization of the initial truncated sphere. The flattened area is in blue (visible due to transparency).

(G) 2D definition of the position of the periclinal wall. The wall is parallel to the line fitted to the boundary of the embryo (orange dashed line). Parameter α indicates the position of the wall (in blue) relative to the most extreme possible positions (in green).

affects a pathway that has not been directly linked to auxin accumulation or response (Ueda et al., 2011), did not show this mode of cell division. To determine whether the auxin-dependent deviation from a geometrically defined default is comparable to a randomization of cell division orientation, we segmented *fass* mutant embryos. *FASS* encodes a protein phosphatase 2A regulatory B subunit (Camilleri et al., 2002) that is required for the formation of the preprophase band, a microtubule structure that forecasts the position of the new division wall (Traas et al., 1995). Hence, cell division planes in the *fass* mutant appear random in 2D (Torres-Ruiz and Jürgens, 1994). Segmentation of *fass* mutant embryos showed that indeed division planes in 3D were randomized (Figures 5B and S4). Despite normal overall embryo size (Figure S2C) and progression (Figure 2B), these random divisions caused aberrant volume partitioning unlike the defined switch induced by *RPS5A≫bdl*, which suggests that the latter is not the result of division randomization.

We then asked how these changes in cell division pattern affected the overall topology of the intercellular network comprising the developing embryo. Embryo patterning was abstracted by generating a network of cell connectivity through the calculation of shared surface areas between neighbor cells. Edges in this network represent shared walls between nodes, which represent cells. The inhibition of auxin response in *RPS5A≫bdl* led to altered cell division patterns and an increase of connectivity in the embryo compared to wild-type (Figures 5F and 5G). This demonstrates that ARF-mediated asymmetric cell divisions act

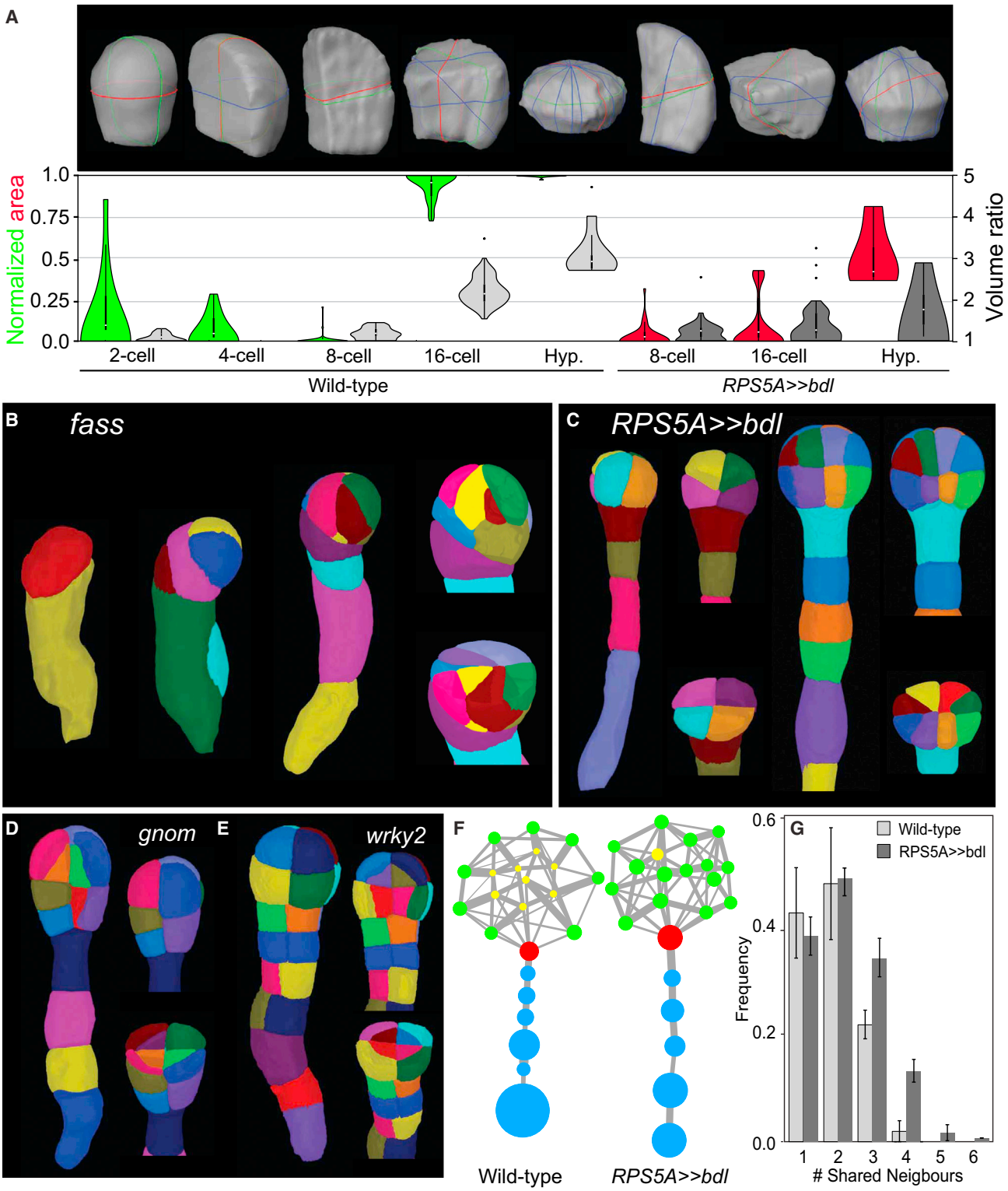

Figure 5. Asymmetric Division through Violating the Default Shortest Wall Rule

(A) Violin plots representing distribution of cell wall areas as a fraction of the smallest (0 on the left y axis) and largest (1 on the left y axis) wall area within the consolidated volume of each pair of sister cells. Wild-type stages are shown in green, and *RPS5A ≫ bdl* in red. The ratios of cell volumes resulting from these divisions are represented in light gray (wild-type) or dark gray (*RPS5A ≫ bdl*), and values are on the right y axis. Representative examples of computation are shown above the graph, where the observed division plane is projected in green, and the global and local minima in red and blue, respectively. Number of cells

(legend continued on next page)

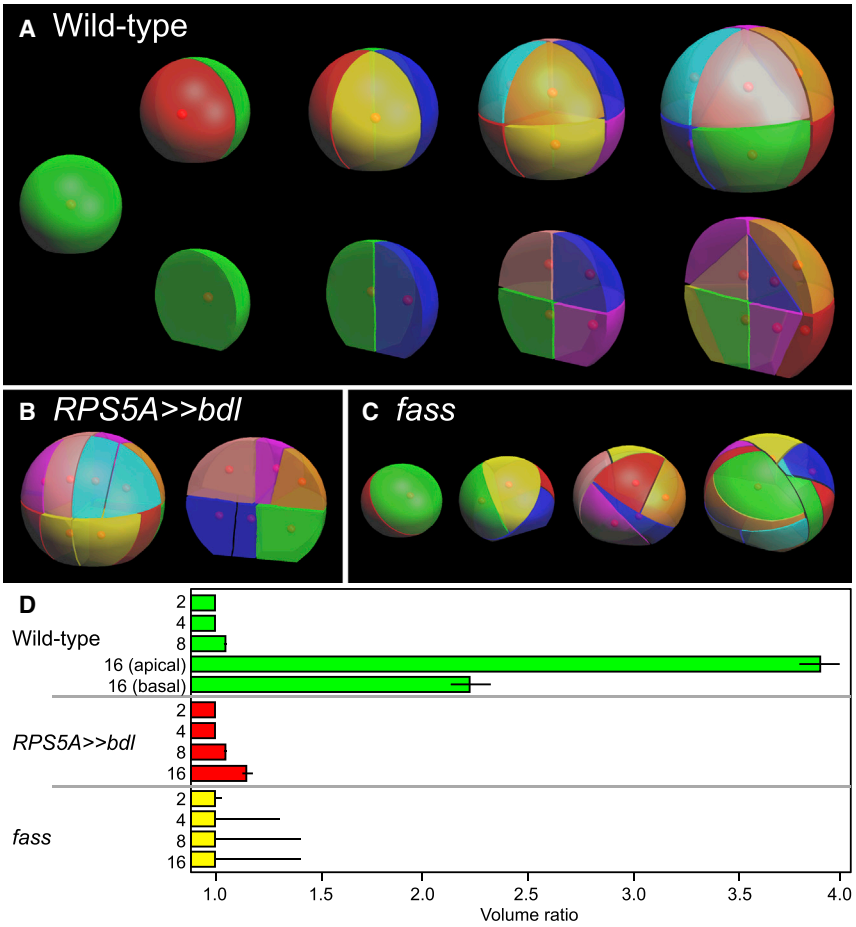

Figure 6. A Growing 3D Embryo Model Recapitulates Normal and Perturbed Development

(A–C) Simulations of embryo growth in 3D under assumptions reflecting rules observed in wild-type (A) (periclinal for division rounds 1 and 4, shortest wall for divisions 2 and 3), *RPS5A ≫ bdl* (B) (shortest wall for all divisions), and *fass* mutant (C) (randomized). Images show successive steps in the simulations. Surface views are shown in (A)–(C) and longitudinal section views are shown in (A) and (B).

(D) Quantification of volume ratios (largest cell volume divided by smallest cell volume) after cell division in simulations of wild-type, *RPS5A ≫ bdl* and *fass* embryos. Values are most likely ratios and ranges indicate the 90% confidence interval.

See also Movies S1, S2, and S3.

to constrain intercellular connectivity in the wild-type embryo. Given the importance of cell-cell communication in cell identity acquisition (Van Norman et al., 2011), we expect such changes in cell division and connectivity in *RPS5A ≫ bdl* have significant effects on cell identity and subsequent pattern formation in this genotype.

3D Model of a Growing Embryo

To determine whether the rules derived from observations in single pairs of cells are capable of explaining development of an entire embryo, we constructed a growing and dividing model of the embryo based on the data acquired. The modeling framework was based on an implementation of cell complexes (Brisson, 1993; Prusinkiewicz and Lane, 2013), a paradigm well suited for the modeling of 3D growing plant tissue with cell division. Since the overall shape and aspect ratio of the embryo does not change significantly until the 16-cell stage (Figure 2A), we assume it to be a truncated sphere (Figure 6A) whose growth is constant and uniform. Divisions occur when cells reach a threshold volume based on observed average cell volumes (Figure 2A). Cell division was modeled by assuming that the division plane is: (1) the smallest area plane going through the geometric center, (2) periclinal and parallel to the embryo surface (e.g., for the 16-cell stage), or (3) a plane of random orientation going through the geometrical center of the cell. Within this framework, the wild-type embryo was modeled by using the shortest wall division for all but the last (i.e., 16-cell stage) division. For the transition to the 16-cell stage, we matched experimental observations by dividing cells according to principle "2" with a volume ratio of 2.2:1 for the basal cells (Figure 3E), and the division walls of the apical cells are close to contiguous to the division walls of the basal cells. This simulation produces a growing embryo with realistic division planes (Figure 6A; Movie S1). We next analyzed whether the model correctly predicted cell volume ratios (Figure 6D). Up to the 8-cell stage, these almost perfectly matched the observed ratios (Figure 3E), although the geometrical asymmetry between apical and basal cells at the 8-cell stage (Figure 3E) was not reproduced (Figures 6A and 6D; Movie S1). We next simulated the *RPS5A ≫ bdl* embryo by allowing all cells to use the default shortest wall rule and found that this faithfully recapitulates the mutant defect both qualitatively (Figure 6B; Movie S2) and in terms of volume ratios (Figure 6D). This mode of division is fundamentally different from

analyzed in wild-type: 2-cell (n = 13), 4-cell (n = 26), 8-cell (n = 34), 16-cell (n = 64), and hypophysis (Hyp.; n = 9); in *RPS5A ≫ bdl*: 8-cell (n = 28), 16-cell (n = 24), and hypophysis (n = 5).

(B) Randomized cell division planes in *fass* mutant embryo. From left to right: 1-cell, 4-cell, and 9-cell (with longitudinal/transverse section).

(C) *RPS5A ≫ bdl* embryos at 6-cell (left) and 16-cell stage (right, including longitudinal and transverse section).

(D and E) Thirteen-cell *gnom* mutant embryo (D) and 16-cell *wrky2* mutant embryo (E).

(F) Connectivity network of wild-type and *RPS5A ≫ bdl* embryos at the 16-cell stage. Each cell is represented as a node with its size reflecting cell volume. Edges represent the shared surface between any two cells, and thickness indicates the relative amount of shared surface area. Blue nodes are suspensor cells, the red node is the hypophysis, green nodes are protoderm (outer), and yellow nodes are the inner cells of the embryo.

(G) Frequency of shared neighbors in wild-type and *RPS5A ≫ bdl* embryos at 16-cell stage (n = 3). Error bars represent SEM.

See also Figure S4.

complete randomization of the division plane (Figures 6C and 6D; Movie S3), which qualitatively resembles the observed *fass* mutant defects (Figures 5B and S4). These simulations showed a much larger variation in cell volume ratios than wild-type or *RPS5A* ≫ *bdl* (Figure 6D), which is in line with the erratic divisions (Figures 5B and S4) and more variable embryo sizes (Figure S2C) observed in the *fass* mutant. The simulations show that the division patterns in 3D can be produced by a minimal set of rules based on cell geometry. It also provides a framework to visualize the impact of cellular division rules on overall embryo development and of developmental regulators on division patterns, and confirms that normal development requires local overriding of the default, geometric cell division rule.

DISCUSSION

During early plant embryogenesis, all major tissue types and their stem cells are generated in a very predictable fashion. In the absence of cell migration, oriented cell division and expansion drive the development of a mature embryo from the fertilized egg cell. Hence, *Arabidopsis* embryogenesis is a good model to study the genetic control of plant development, and several important regulators have been identified (Tzafrir et al., 2004; Lau et al., 2012). Thus far, plant embryogenesis has been described and studied in 2D, which left important questions unanswered. Here, we have generated a complete description of cellular patterns and volumes in 3D for all stages up to the heart stage, at which the embryonic leaves (cotyledons), shoot and root meristems, and hypocotyl are established. We use this description to address questions about control of oriented cell division, lineage patterns, asymmetric division, and the genetic and geometric influence on division orientation.

A surprising finding is that the orientation of the first division of the embryonic cell after zygote division is not random relative to the symmetry axis of the surrounding seed. Rather, division planes fall within a narrow range of 45°. Previously, it had been shown using marked sector analysis that the cell lineages that give rise to the left and right cotyledon are separated very early, perhaps before the 2- to 4-cell stage (Saulsberry et al., 2002). Therefore, our findings suggest that the orientation of the cotyledons within the seed is determined by tight control of the first embryonic cell division. This early determination could be biologically meaningful as the seed cavity that houses the embryo has a very defined shape, and the embryo axis and cotyledons occupy precise locations in this cavity at maturity. The early determination of cell division orientation, by positioning the axis of bisymmetry, could help to ensure that cotyledons are correctly positioned in the mature seed. The orienting influence at the first embryonic cell division is entirely unknown, and it is unclear whether it is of chemical or physical nature. What is clear though is that either the maternal tissues exert an effect on division orientation in the embryo or the developmental trajectory of the ovule prior to fertilization predisposes later embryonic cell division. Interestingly, this bias is not limited to the first cell, as later divisions in the apical protoderm are also biased to occur perpendicular to the left-right axis (Figure 3F). The testable prediction that follows from this finding is that mutations that affect seed coat structure or ovule development before fertilization will also cause abnormalities in embryonic cell division orientation, and perhaps in cotyledon positioning.

Oriented cell divisions are a major morphogenetic driver in plant development. We have used the *Arabidopsis* embryo to address how pattern and shape are genetically controlled in a growing 3D structure. Our work provides quantitative 3D data on the effect of cell shape on division planes, supporting theories of plant cell division proposed more than a century ago. Interestingly, many cells divide in unequal volumes, creating asymmetry that we find to correlate with the formation of daughter cells with distinct identity. Invariably, these divisions depart from the default geometric rule. By genetic perturbation, we demonstrate that auxin transcriptional response is required to override this default rule to allow asymmetric division.

In the 8-cell embryo, this deviation from the default allows the separation of outer and inner cells, which will form protoderm and inner cell types, respectively. The finding that auxin response inhibition perturbs this division suggests that there might be a direct link between auxin response and protoderm formation. By definition, any division in these cells that is not perpendicular to the surface of the embryo will fail to separate outside and inside. Therefore, auxin response is formally required for this step. However, later *RPS5A* ≫ *bdl* embryos do form a separate outer layer (Rademacher et al., 2012), which suggests that auxin response is not critically required for epidermis formation. It will be interesting to see whether the link between auxin-dependent transcription (as inhibited by bdl) and the epidermal specification process is direct, or if it follows from the geometric constraints of the 8-cell embryo.

Correlations between division asymmetry and differential cell fate determination have been shown in other systems, such as the stomatal lineage (Robinson et al., 2011) and lateral root initiation (De Smet et al., 2008). We extend these findings to show that in the early embryo, 3D asymmetry is a reliable indicator of differential cell specification. An important question is how critical these asymmetries are and if they are utilized by pattern formation pathways. Division of a cellular volume by a ratio of 1:2.2 (at the 16-cell stage) causes significant absolute differences in the number of organelles and molecules inherited, but concentrations of molecules will be equal in the two daughter cells. Depending on whether concentrations or numbers matter, such differences can have significant consequences. Future studies should address if this partitioning mechanism is exploited by embryo patterning regulators such as, for example, the epidermal specifier ATML1 (Lu et al., 1996; Takada and Jürgens, 2007; Takada et al., 2013).

This work provides a conceptual framework and several genetic, microscopic, and computational tools to understand the cellular basis of patterned 3D growth and to rationalize normal, as well as perturbed, development. An interesting prediction following from our model is that the ''cleavage-like'' divisions that lead to the 8-cell embryo might require no input other than a general coupling of cell geometry to a ''shortest wall'' principle. In contrast, an alternative model where cell division orientation is actively switched after every division will require more regulatory input.

An interesting question is how general this mechanism is. We show that loss of auxin response causes a switch to the shortest wall rule in various differently shaped cells in the early embryo.

Hence, when stripped of the capacity to respond to auxin, embryo cells use only geometric cues to orient their cell division plane. In support of a role for auxin in overriding the default shortest wall rule, each of these cells shows a clear transcriptional auxin response as reported by the *DR5-GFP* marker (Friml et al., 2003). In other contexts, auxin-regulated development involves divisions that might not be approximated by deviations from the default rule. Examples include the initiation of organ primordia in floral meristems (Heisler et al., 2005) or along the main root (Lucas et al., 2013). Clearly, the formative potential of every division in the embryo urges tight regulatory mechanisms that operate at the level of individual cells. Such cell-level control might not be equally important in developmental processes that are regulated at the level of cell populations. We envision that similar 3D analyses and simulations of other, auxin-dependent cell divisions will inform how general this mechanism is.

Given the apparent geometric input into cell division plane orientation, it is evident that physical properties of cells will play an important role. In animal systems, both supracellular and cellular models for division plane orientation have been proposed. In *Drosophila*, a packing constraint at tissue level was shown to influence cell division orientation (Gibson et al., 2011), and in sea urchin, microtubule organization and hence division plane were directly influenced by cell geometry (Minc et al., 2011). It is likely that tensile forces generated by the microtubule cytoskeleton (Lloyd, 1991; Besson and Dumais, 2011), as well as mechanical properties of pre-existing cell walls, will play an important role in any mechanism that couples cell shape to a "shortest wall" principle. As *bdl* misexpression primarily impacts transcription through inhibiting DNA-binding ARF transcription factors (Rademacher et al., 2012), the identification of auxin-dependent transcriptional networks will be an important next step in understanding the control of oriented cell division.

EXPERIMENTAL PROCEDURES

Plant Material

Plants were grown at a constant temperature of 22°C in a 16 hr light/8 hr dark cycle. The following mutant lines of *Arabidopsis* have been described previously: *fass* mutant (*fass 325-23*, *fass 226-32*; Torres-Ruiz and Jürgens, 1994), *wrky2-1* (Ueda et al., 2011), and *gnom* (Mayer et al., 1993). The *pRPS5A≫bdl* embryos that ubiquitously misexpress a nondegradable version of the auxin response inhibitor *bodenlos/iaa12* were generated by crossing homozygous *UAS-bdl* (Weijers et al., 2006) pollen onto homozygous *RPS5A-GAL4* (Weijers et al., 2003) pistils. Wild-types were Columbia (*RPS5A-GAL4*; *UAS-bdl*; *wrky2-1*) or Landsberg *erecta* (*fass 325-23*; *fass 226-32*; *gnom*). While *RPS5A-GAL4* × *UAS-bdl* crossing yielded 100% mutant embryos, all other mutants segregate 25% homozygous embryos, which were identified based on abnormal morphology.

Fluorescent Staining and Microscopy

Embryos were imaged live in 1 μM FM4-64 in 0.5× Murashige and Skoog medium or stained by the modified Pseudo-Schiff propidium iodide (PI) staining method (Truernit et al., 2008) with the following modifications: ovules were dissected from siliques before fixation and fixed ovules were treated with periodic acid for 60–80 min and stained with 300 μM of PI for 1–2 hr. For the staining of embryos at postglobular stages, embryos were dissected from ovules using fine tungsten needles after staining. The stained ovules/embryos were mounted in a drop of chloral hydrate in a well generated by pieces of glass coverslip and observed by confocal microscopy for taking z-stack images. A series of 2D confocal images were recorded at 0.1 μm intervals using a Zeiss LSM510 microscope or Leica SP5-II system, with excitation at 561 nm and detection at 600–700 nm.

For differential interference contrast (DIC) microscopy, ovules were cleared in a chloral hydrate:water:glycerol mixture (w:v:v) and imaged on a Leica DMR microscope with DIC optics.

Optical deformation by the microscope was determined by using fluorescent beads of calibrated diameter (15 μm beads: PS-speck Microscope Point Source Kit, Molecular Probes; 90–180 μm beads: P6 beads, biogel).

For determining the orientation of the first embryonic division relative to the seed axis, z-stacks were generated of entire seeds containing 2-cell embryos. Seeds were aligned in MorphoGraphX such that the symmetry plane was aligned with the X-Y plane of the viewer. A plane was then placed through the division wall of the apical cell. This enabled the extraction of the angle between the symmetry plane and the division wall.

Cell Segmentation and Shape Extraction

The segmentation and shape extraction were done using MorphoGraphX (http://www.MorphoGraphX.org), an open source software package we developed for the visualization, segmentation, and analysis of 3D images (Kierzkowski et al., 2012). The images were first trimmed using clipping planes to remove most of the unwanted tissues. Then, the images were smoothed with a 3D Gaussian filter of radius typically 0.6 μm. After this, the autoseeded morphologic watershed algorithm from the Insight toolkit was used to segment the cells. The cell shape was then extracted using a modified marching cube algorithm with a cube size of 1 μm.

Computational Methods

Details about all computation, including the analysis of bead deformation, volume computation, cell classification, division plane detection, simulation, cell structure representation, division frequency estimation, division surface estimation, simulations of division planes, and cell connectivity networks are described in the Supplemental Computational Methods.

SUPPLEMENTAL INFORMATION

Supplemental Information includes Supplemental Computational Methods, four figures, and three movies and can be found with this article online at http://dx.doi.org/10.1016/j.devcel.2014.02.002.

AUTHOR CONTRIBUTIONS

S.Y. optimized imaging procedures and collected all experimental data. P.B.d.R. and R.S.S. developed MorphoGraphX software. P.B.d.R. performed all computational analysis and developed 3D simulations with the help of B.L. and P.P. Cellular network analysis was done by G.W.B. R.S.S. and D.W. conceived the study and supervised the project. S.Y., P.B.d.R., R.S.S., and D.W. wrote the manuscript with input from all other authors.

ACKNOWLEDGMENTS

We thank Gerd Jürgens, Ramon Torres-Ruiz, and Thomas Laux for mutant seeds, Cris Kuhlemeier for support and discussions, Jan Willem Borst (Microspectroscopy Center Wageningen) for advice on microscopy, and Bert De Rybel and Jos Wendrich for comments on the manuscript. This work was supported by the Earth and Life Sciences Council (ALW) of the Netherlands Organization for Scientific Research (NWO; ALW-820.02.019 to D.W.), the European Research Council (starting grant "CELLPATTERN"; contract no. 281573 to D.W.), the Swiss National Science Foundation (CR3213_132586 and CR3213_143833 to R.S.S.), SystemsX.ch ("Plant Growth" RTD to R.S.S.), the Natural Sciences and Engineering Research Council of Canada (NSERC, Discovery Grant 130084-2008 to P.P. and Postgraduate Fellowship to B.L.) and a Birmingham Fellowship to G.W.B.

Received: November 26, 2013
Revised: January 20, 2014
Accepted: February 4, 2014
Published: March 27, 2014

REFERENCES

Besson, S., and Dumais, J. (2011). Universal rule for the symmetric division of plant cells. Proc. Natl. Acad. Sci. USA *108*, 6294–6299.

Bougourd, S., Marrison, J., and Haseloff, J. (2000). Technical advance: an aniline blue staining procedure for confocal microscopy and 3D imaging of normal and perturbed cellular phenotypes in mature Arabidopsis embryos. Plant J. *24*, 543–550.

Brisson, E. (1993). Representing geometric structures in d dimensions: topology and order. Discrete Comput. Geom. *9*, 387–426.

Camilleri, C., Azimzadeh, J., Pastuglia, M., Bellini, C., Grandjean, O., and Bouchez, D. (2002). The Arabidopsis TONNEAU2 gene encodes a putative novel protein phosphatase 2A regulatory subunit essential for the control of the cortical cytoskeleton. Plant Cell *14*, 833–845.

De Smet, I., and Beeckman, T. (2011). Asymmetric cell division in land plants and algae: the driving force for differentiation. Nat. Rev. Mol. Cell Biol. *12*, 177–188.

De Smet, I., Vassileva, V., De Rybel, B., Levesque, M.P., Grunewald, W., Van Damme, D., Van Noorden, G., Naudts, M., Van Isterdael, G., De Clercq, R., et al. (2008). Receptor-like kinase ACR4 restricts formative cell divisions in the Arabidopsis root. Science *322*, 594–597.

Dupuy, L., Mackenzie, J., and Haseloff, J. (2010). Coordination of plant cell division and expansion in a simple morphogenetic system. Proc. Natl. Acad. Sci. USA *107*, 2711–2716.

Errera, L. (1888). Über zellformen und seifenblasen. Bot. Zentralbl. *34*, 395–398.

Federici, F., Dupuy, L., Laplaze, L., Heisler, M., and Haseloff, J. (2012). Integrated genetic and computation methods for in planta cytometry. Nat. Methods *9*, 483–485.

Fernandez, R., Das, P., Mirabet, V., Moscardi, E., Traas, J., Verdeil, J.L., Malandain, G., and Godin, C. (2010). Imaging plant growth in 4D: robust tissue reconstruction and lineaging at cell resolution. Nat. Methods *7*, 547–553.

Friml, J., Vieten, A., Sauer, M., Weijers, D., Schwarz, H., Hamann, T., Offringa, R., and Jürgens, G. (2003). Efflux-dependent auxin gradients establish the apical-basal axis of Arabidopsis. Nature *426*, 147–153.

Gibson, W.T., Veldhuis, J.H., Rubinstein, B., Cartwright, H.N., Perrimon, N., Brodland, G.W., Nagpal, R., and Gibson, M.C. (2011). Control of the mitotic cleavage plane by local epithelial topology. Cell *144*, 427–438.

Hamann, T., Mayer, U., and Jürgens, G. (1999). The auxin-insensitive bodenlos mutation affects primary root formation and apical-basal patterning in the Arabidopsis embryo. Development *126*, 1387–1395.

Hamann, T., Benkova, E., Bäurle, I., Kientz, M., and Jürgens, G. (2002). The Arabidopsis BODENLOS gene encodes an auxin response protein inhibiting MONOPTEROS-mediated embryo patterning. Genes Dev. *16*, 1610–1615.

Hardtke, C.S., and Berleth, T. (1998). The Arabidopsis gene MONOPTEROS encodes a transcription factor mediating embryo axis formation and vascular development. EMBO J. *17*, 1405–1411.

Heisler, M.G., Ohno, C., Das, P., Sieber, P., Reddy, G.V., Long, J.A., and Meyerowitz, E.M. (2005). Patterns of auxin transport and gene expression during primordium development revealed by live imaging of the Arabidopsis inflorescence meristem. Curr. Biol. *15*, 1899–1911.

Hofmeister, W. (1863). Zusätze und berichtigungen zu den 1851 veröffentlichten untersuchungen der entwicklung höherer krytogamen. Jahrb. Wiss. Bot. *3*, 259–293.

Jürgens, G., and Mayer, U. (1994). Arabidopsis. In EMBRYOS Colour Atlas of Development, J.B.L. Bard, ed. (London: Wolfe Publishing), pp. 7–21.

Kierzkowski, D., Nakayama, N., Routier-Kierzkowska, A.L., Weber, A., Bayer, E., Schorderet, M., Reinhardt, D., Kuhlemeier, C., and Smith, R.S. (2012). Elastic domains regulate growth and organogenesis in the plant shoot apical meristem. Science *335*, 1096–1099.

Kimmel, C.B., and Law, R.D. (1985). Cell lineage of zebrafish blastomeres. I. Cleavage pattern and cytoplasmic bridges between cells. Dev. Biol. *108*, 78–85.

Knoblich, J.A. (2008). Mechanisms of asymmetric stem cell division. Cell *132*, 583–597.

Kwiatkowska, D. (2004). Structural integration at the shoot apical meristem: models, measurements, and experiments. Am. J. Bot. *91*, 1277–1293.

Lau, S., Slane, D., Herud, O., Kong, J., and Jürgens, G. (2012). Early embryogenesis in flowering plants: setting up the basic body pattern. Annu. Rev. Plant Biol. *63*, 483–506.

Lloyd, C.W. (1991). How does the cytoskeleton read the laws of geometry in aligning the division plane of plant cells? Development *113* (*Suppl 1*), 55–65.

Lu, P., Porat, R., Nadeau, J.A., and O'Neill, S.D. (1996). Identification of a meristem L1 layer-specific gene in Arabidopsis that is expressed during embryonic pattern formation and defines a new class of homeobox genes. Plant Cell *8*, 2155–2168.

Lucas, M., Kenobi, K., von Wangenheim, D., Vobeta, U., Swarup, K., De Smet, I., Van Damme, D., Lawrence, T., Peret, B., Moscardi, E., et al. (2013). Lateral root morphogenesis is dependent on the mechanical properties of the overlaying tissues. Proc. Natl. Acad. Sci. USA *110*, 5229–5234.

Mansfield, S.G., and Briarty, L.G. (1991). Early embryogenesis in *Arabidopsis thaliana*. II. The developing embryo. Can. J. Bot. *69*, 461–476.

Mayer, U., Torres-Ruiz, R.A., Berleth, T., Misera, S., and Jürgens, G. (1991). Mutations affection body organization in the *Arabidopsis* embryo. Nature *353*, 402–407.

Mayer, U., Büttner, G., and Jürgens, G. (1993). Apical-basal pattern formation in the *Arabidopsis* embryo: studies on the role of the *GNOM* gene. Development *117*, 149–162.

Minc, N., Burgess, D., and Chang, F. (2011). Influence of cell geometry on division-plane positioning. Cell *144*, 414–426.

Mulnard, J.G. (1967). Analyse microcinématographique du développement de l'oeuf de souris du stade II au blastocyste [Microcinematographic analysis of the mouse egg development from stage 2 to the blastocyst]. Arch. Biol. (Liege) *78*, 107–139.

Nakielski, J. (2000). Tensorial model for growth and cell division in the shoot apex. In Pattern Formation in Biology, Vision and Dynamics, A. Carbone, M. Gromov, and P. Prusinkiewicz, eds. (World Scientific), pp. 252–286.

Prusinkiewicz, P., and Lane, B. (2013). Modeling morphogenesis in multicellular structures with cell complexes and L-systems. In Pattern Formation in Morphogenesis, V. Capasso, M. Gromov, A. Harel-Bellan, N. Morozova, and L.L. Pritchard, eds. (Springer), pp. 137–151.

Rademacher, E.H., Möller, B., Lokerse, A.S., Llavata-Peris, C.I., van den Berg, W., and Weijers, D. (2011). A cellular expression map of the Arabidopsis AUXIN RESPONSE FACTOR gene family. Plant J. *68*, 597–606.

Rademacher, E.H., Lokerse, A.S., Schlereth, A., Llavata-Peris, C.I., Bayer, M., Kientz, M., Freire Rios, A., Borst, J.W., Lukowitz, W., Jürgens, G., and Weijers, D. (2012). Different auxin response machineries control distinct cell fates in the early plant embryo. Dev. Cell *22*, 211–222.

Robinson, S., Barbier de Reuille, P., Chan, J., Bergmann, D., Prusinkiewicz, P., and Coen, E. (2011). Generation of spatial patterns through cell polarity switching. Science *333*, 1436–1440.

Sachs, J. (1878). Über die anordnung der zellen in jüngsten pflanzenteilen. Arb. Bot. Inst. Würzburg *2*, 46–104.

Sahlin, P., and Jönsson, H. (2010). A modeling study on how cell division affects properties of epithelial tissues under isotropic growth. PLoS One *5*, e11750.

Saulsberry, A., Martin, P.R., O'Brien, T., Sieburth, L.E., and Pickett, F.B. (2002). The induced sector Arabidopsis apical embryonic fate map. Development *129*, 3403–3410.

Scheres, B., Wolkenfelt, H., Willemsen, V., Terlouw, M., Lawson, E., Dean, C., and Weisbeek, P. (1994). Embryonic origin of the Arabidopsis primary root and root meristem initials. Development *120*, 2475–2487.

Sena, G., Wang, X., Liu, H.Y., Hofhuis, H., and Birnbaum, K.D. (2009). Organ regeneration does not require a functional stem cell niche in plants. Nature *457*, 1150–1153.

Smith, R.S., Guyomarc'h, S., Mandel, T., Reinhardt, D., Kuhlemeier, C., and Prusinkiewicz, P. (2006). A plausible model of phyllotaxis. Proc. Natl. Acad. Sci. USA *103*, 1301–1306.

Steinmann, T., Geldner, N., Grebe, M., Mangold, S., Jackson, C.L., Paris, S., Gälweiler, L., Palme, K., and Jürgens, G. (1999). Coordinated polar localization of auxin efflux carrier PIN1 by GNOM ARF GEF. Science *286*, 316–318.

Stoma, S., Lucas, M., Chopard, J., Schaedel, M., Traas, J., and Godin, C. (2008). Flux-based transport enhancement as a plausible unifying mechanism for auxin transport in meristem development. PLoS Comput. Biol. *4*, e1000207.

Takada, S., and Jürgens, G. (2007). Transcriptional regulation of epidermal cell fate in the Arabidopsis embryo. Development *134*, 1141–1150.

Takada, S., Takada, N., and Yoshida, A. (2013). ATML1 promotes epidermal cell differentiation in Arabidopsis shoots. Development *140*, 1919–1923.

Torres-Ruiz, R.A., and Jürgens, G. (1994). Mutations in the FASS gene uncouple pattern formation and morphogenesis in Arabidopsis development. Development *120*, 2967–2978.

Traas, J., Bellini, C., Nacry, P., Kronenberger, J., Bouchez, D., and Caboche, M. (1995). Normal differentiation patterns in plants lacking microtubular preprophase bands. Nature *375*, 676–677.

Truernit, E., Bauby, H., Dubreucq, B., Grandjean, O., Runions, J., Barthélémy, J., and Palauqui, J.C. (2008). High-resolution whole-mount imaging of three-dimensional tissue organization and gene expression enables the study of phloem development and structure in Arabidopsis. Plant Cell *20*, 1494–1503.

Tzafrir, I., Pena-Muralla, R., Dickerman, A., Berg, M., Rogers, R., Hutchens, S., Sweeney, T.C., McElver, J., Aux, G., Patton, D., and Meinke, D. (2004). Identification of genes required for embryo development in Arabidopsis. Plant Physiol. *135*, 1206–1220.

Ueda, M., Zhang, Z., and Laux, T. (2011). Transcriptional activation of Arabidopsis axis patterning genes WOX8/9 links zygote polarity to embryo development. Dev. Cell *20*, 264–270.

Van Norman, J.M., Breakfield, N.W., and Benfey, P.N. (2011). Intercellular communication during plant development. Plant Cell *23*, 855–864.

Weijers, D., Van Hamburg, J.P., Van Rijn, E., Hooykaas, P.J., and Offringa, R. (2003). Diphtheria toxin-mediated cell ablation reveals interregional communication during Arabidopsis seed development. Plant Physiol. *133*, 1882–1892.

Weijers, D., Schlereth, A., Ehrismann, J.S., Schwank, G., Kientz, M., and Jürgens, G. (2006). Auxin triggers transient local signaling for cell specification in Arabidopsis embryogenesis. Dev. Cell *10*, 265–270.

Wolters, H., Anders, N., Geldner, N., Gavidia, R., and Jürgens, G. (2011). Coordination of apical and basal embryo development revealed by tissue-specific GNOM functions. Development *138*, 117–126.